ACS APPLIED MATERIALS & INTERFACES

Energy, Environmental, and Catalysis Applications

Structure-Electronic Property Relationships of 2D Ruddlesden-Popper Tin- and Lead-based Iodide Perovskites

Nourdine Zibouche, and Saiful Islam

ACS Appl. Mater. Interfaces, **Just Accepted Manuscript** • DOI: 10.1021/acsami.0c03061 • Publication Date (Web): 11 Mar 2020

Just Accepted

Structure–Electronic Property Relationships of 2D Ruddlesden-Popper Tin- and Lead-based Iodide Perovskites

Nourdine Zibouche* and M. Saiful Islam*

Department of Chemistry, University of Bath, Bath BA2 7AY, UK

E-mail: n.zibouche@bath.ac.uk; m.s.islam@bath.ac.uk
Phone: +44(0)1225 384938

Abstract

Two–dimensional (2D) halide perovskites are receiving considerable attention for applications in photovoltaics, largely due to their versatile composition and superior environmental stability over 3D perovskites, but show much lower power conversion efficiencies. Hence, further understanding of the structure–property relationships of these 2D materials is crucial for improving their photovoltaic performance. Here, we investigate by means of first-principles calculations the structural and electronic properties of 2D lead and tin Ruddlesden–Popper perovskites with general formula $(BA)_2A_{n-1}B_nI_{3n+1}$, where BA is the butylammonium organic spacer, A is either methylammonium (MA) or formamidinium (FA) cations, B represents Sn or Pb atoms, and n is the number of layers (n = 1, 2, 3, and 4). We show that the band gap progressively increases as the number of layers decreases in both Sn- and Pb-based materials. Through substituting MA by FA cations, the band gap slightly opens in the Sn systems and narrows in the Pb systems. The electron and hole carriers show small effective masses, which are lower than those of the corresponding 3D perovskites, suggesting high carrier mobilities. The structural distortion associated with the orientation of the MA or FA cations in the inorganic layers is found to be the driving force for the induced Rashba spin-splitting bands in the systems with more than one layer. From band alignment diagrams, the transfer process of the charge carriers in the 2D perovskites is found to be from smaller to higher number of layers n for electrons and oppositely for holes, in excellent agreement with experimental studies. We also find that when interfaced with 3D analogues, the 2D perovskites could function as hole transport materials.

Keywords

Halide Perovskites, Tin, Lead, Ruddlesden–Popper, DFT, band alignment

1 Introduction

Halide perovskites have recently gained considerable interest for applications in photovoltaics and solar cells owing to their exceptional physical and chemical properties.[1–3] In particular, Pb-based halide perovskites have attained power conversion efficiencies (PCEs) exceeding 25%.[4] However, these materials have stability problems, resulting in impaired long-term performance of perovskite solar cells,[5–7] as well as the toxicity issue of Pb, which may hinder practical applications.[8–11] Sn-based perovskite materials seem to be amongst the most

promising Pb–free alternatives,[12–22] although they also suffer from oxidation of Sn^{2+} to Sn^{4+}, resulting in poor stability.[18,23,24]

Recent studies showed that the incorporation of 2D layered halide perovskites alongside the 3D perovskites effectively enhanced the performance of the perovskite solar cell devices.[25–30] The most well-known 2D perovskites are the so-called Ruddlesden-Popper compounds with general formula $A'_2A_{n-1}B_nX_{3n+1}$, where A' are organic cations, such as phenylethylammonium (PEA) or butylammonium (BA) used as spacing layers for separating the perovskite units, A are methylammonium (MA) or formamidinium (FA) cations within the perovskites units, B refers to the metal cations such as Pb, Sn or Ge, X are the halide anions (Cl, Br, or I), and n corresponds to the number of the inorganic layers formed by the BX_6 octahedra. These 2D perovskites show a wide range of appealing properties,[31–39] including tunable band gaps with the number of layers, small charge-carrier effective masses, and good stability when exposed to moisture and radiation.[40–47] The crystal structures of these materials consist of stacks formed by alternating 2D strongly bonded inorganic layers, resembling the structure of the 3D halide perovskites, such as $MAPbI_3$, and weakly bonded organic layers.

Within solar cells, 2D perovskites can be used as light absorbers or can be integrated for the reinforcement of the photoactive 3D perovskites. Smith et *al.*[48] reported the first perovskite solar cell device fabricated using exclusively a 2D perovskite, displaying a PCE of 4.73% and an open-circuit voltage (V_{oc}) of 1.18 V.[48] Tsai et *al.*[49] recorded a PCE of 12.52% using $(BA)_2(MA)_{n-1}Pb_nI_{3n+1}$ (n = 3, 4), and showed enhanced environmental stability compared to their 3D counterparts.[49] Using quasi–2D perovskites based on Pb, Zheng et *al.* demonstrated an efficiency of 17.40% with high quality films and excellent resistance to moisture.[50] Wang et *al.* intercalated butylammonium (BA) cations as a spacing layer in a 3D Pb-based perovskite to form a mixed 2D/3D heterostructure, and achieved a record PCE of 20.6%.[51]

However, these 2D perovskites have not yet achieved the efficiencies of their 3D counterparts. It is, therefore, necessary to further explore the structure-property relationships of these 2D materials to understand the changes in their electronic properties with layer thickness, the role of the organic cations in the perovskite-like units, and to identify the features that can improve their use in photovoltaic applications as the main light absorbing materials or in combination with 3D parent perovskites.

In this work, density functional theory methods are used to investigate the 2D Ruddlesden−Popper perovskites based on lead and tin with the general formula of $(BA)_2A_{n-1}B_nI_{3n+1}$, where BA is the butylammonium ($CH_3(CH_2)_3NH_3$) spacer, A refers to MA (CH_3NH_3) or FA ($CH(NH_2)_2$) cations, B is Pb or Sn, and n varies from 1 to 4, which extends our recent studies on 3D halide perovskites.[52–55] We examine the structural and electronic properties of these Sn- and Pb-based systems by varying the number of layers n. We also examine the effect of the organic A cation in the perovskite units by substituting MA with FA cations, since it has been shown recently that mixed A cations results in better stability and efficiency of solar cell devices.[56,57]

We show that the band gaps typically decrease with increasing layer thickness n and converge towards those of the 3D perovskites, as well as exhibiting low charge-carrier effective masses. The structural arrangement of MA or FA cations in the perovskite cages are found to induce Rashba splitting in the band structures for systems with $n > 1$. The band level alignment provides the transport mechanism of photogenerated charge carriers within the 2D materials and the type of charge extraction from their 3D counterparts.

2 Methods

Calculations were carried out using density functional theory (DFT)[58] as implemented in the Quantum Espresso simulation package.[59,60] The Kohn-Sham wave-functions and energies were calculated using the PBEsol exchange-correlation functional,[61] and a plane-wave basis

with energy and charge density cutoffs of 40 and 400 Ry, respectively. Ultra-soft pseudopotentials[62,63] were used to describe the core-valence interactions. The structural relaxation is performed until the force on each atom is smaller than 0.01 eV/Å. The Brillouin Zone integration was sampled following the Monkhorst-Pack scheme,[64] using $4\times4\times2$ ($4\times2\times4$ for $n = 1$) and $6\times6\times1$ ($6\times1\times6$ for $n = 1$) k-point grids for the ionic optimization and the electronic structure calculations, respectively. Full relativistic calculations were accounted by the inclusion of spin-orbit coupling (SOC). We have also examined the effect of van der Waals (vdW) corrections in simulating these halide perovskites (details in the SI, section S1) . We found that the geometries and the electronic structure remain unaffected, and therefore, in the following work, vdW corrections are not included.

For the calculation of the work–function and a better description of the energy level alignment between the 2D and 3D perovskites, we performed hybrid functional calculations at the PBE0 level,[65,66] which has been shown to provide reliable values for the ionization and affinity potentials.[67] The crystal structures of these 2D perovskites include several hundreds of atoms and work–function calculations with plane-wave methods would require prohibitive computational resources. To reduce the computational cost, we used the Crystal17 code,[68] which employs localized basis functions and does not require artificial periodicity along the out–of–plane direction to the slab. The work–function is then calculated following the method proposed by Doll.[69] For comparison, we have also calculated the band gaps, work–functions and energy band alignment diagram using HSE for Pb-based systems with MA cations. Details on the calculation of the work–functions and the energy band alignment are given in section S2 of the supporting information.

3 Results & discussion

3.1 Structural properties

Sn- and Pb-based 2D perovskites ($(BA)_2A_{n-1}B_nI_{3n+1}$) with butylammonium (BA) as the organic separating layers have been characterized by single crystal X-ray diffraction and are found to adopt orthorhombic systems with space groups *Pbca* and *Cc2m*.[32,70] The inorganic layers of these 2D perovskites resemble the parent 3D perovskite structures, such as $MAPbI_3$ and $MASnI_3$. They are mainly synthesized with the MA cation occupying the cages between the PbI_6 or SnI_6 octahedra for different numbers of layers n ranging from 1 to 4, as shown in Figure 1. In this study, the initial MA–based structures are taken from diffraction experiments.[32,70] We also investigate 2D perovskites with the FA cation substituting the MA cation, as this was shown to affect the optoelectronic properties of the 3D halide perovskites.[71]

The lattice parameters of the fully optimized Sn– and Pb–based structures are shown in Table 1 for systems with MA cations and in Table S1 for Sn/Pb systems with FA cations. Our calculated results agree well with the available experimental[32,70] and theoretical[72] data for both Pb– and Sn–based structures with MA cations. For systems with FA cations, no experimental data are available for direct comparison. In the case of Pb- and Sn-based 2D perovskites with MA cations, the average lattice constants in the in-plane directions of the layers ($(a + b)/2$ for $n = 1$, and $(a + c)/2$ for $n = 2 - 4$) are slightly smaller than those corresponding experimental structures, whereas the out-of-plane lattice constants are relatively larger, for even number ($n = 2$ and 4) and shorter for odd numbers ($n = 1$ and 3) compared to the experimental results. By replacing MA with FA cations in the Pb and Sn systems with $n > 1$, the average lattice constants become larger, while the out-of-plane lattice constants are reduced for $n = 2$ and 4 and enlarged for $n = 3$. For the Pb and Sn structures with an even number of layers ($n = 2, 4$), the angles between the lattice vectors deviate from 90°

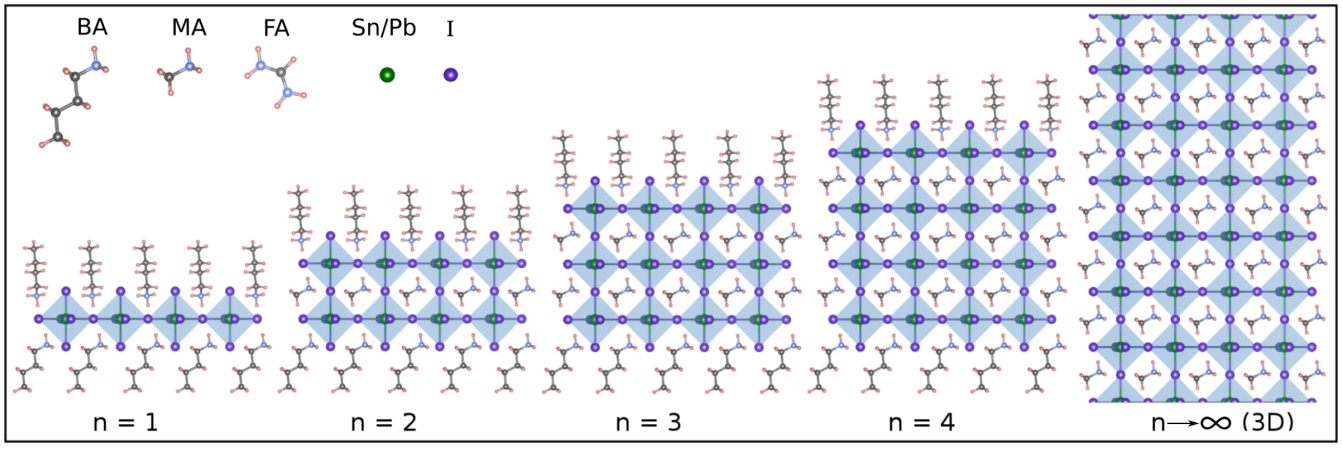

Figure 1: Crystal structures of a typical 3D perovskite and 2D Ruddlesden–Popper perovskites $(BA)_2A_{n-1}B_nI_{3n+1}$, for n = 1–4. BA denotes the organic alkylammonium spacer, MA and FA are, respectively, the organic methylammonium and formamidinium cations in the perovskite units, Pb and Sn are the metal cations, and I represents the iodine anions.

Table 1: Comparison of experimental[32,70] and computed structural parameters of $(BA)_2(MA)_{n-1}Sn_nI_{3n+1}$ and $(BA)_2MA_{n-1}Pb_nI_{3n+1}$

Parameters	(n = 1)		(n = 2)		(n = 3)		(n = 4)	
	$(BA)_2SnI_4$		$(BA)_2MASn_2I_7$		$(BA)_2(MA)_2Sn_3I_{10}$		$(BA)_2(MA)_3Sn_4I_{13}$	
	calc.	exp.	calc.	exp.	calc.	exp.	calc.	exp.
a (Å)	8.657	8.837	8.670	8.858	8.890	8.860	8.900	—
b (Å)	8.505	8.619	41.736	39.497	51.033	51.870	65.460	64.29
c (Å)	27.774	27.562	8.527	8.776	8.639	8.790	8.530	—
α	90°	90°	88.39°	90°	90°	90°	89.95°	90°
β	90°	90°	89.47°	90°	90°	90°	89.97°	90°
γ	90°	90°	89.67°	90°	90°	90°	89.94°	90°
	$(BA)_2PbI_4$		$(BA)_2MAPb_2I_7$		$(BA)_2(MA)_2Pb_3I_{10}$		$(BA)_2(MA)_3Pb_4I_{13}$	
	calc.	exp.	calc.	exp.	calc.	exp.	calc.	exp.
a (Å)	8.680	8.863	8.655	8.947	9.000	8.928	9.028	8.927
b (Å)	8.560	8.682	41.770	39.350	51.205	51.959	66.965	64.380
c (Å)	28.140	27.570	8.574	8.860	8.770	8.878	8.600	8.882
α	90°	90°	88.42°	90°	90°	90°	90.40°	90°
β	90°	90°	89.53°	90°	90°	90°	89.96°	90°
γ	90°	90°	89.71°	90°	90°	90°	90.35°	90°

by up to 1.87%. Hence, these systems prefer lower symmetry structures and adopt triclinic instead of orthorhombic crystals as compared to experimental structures.[32,70] This is probably because such systems are non-centrosymmetric compared to the systems with an odd number of layers. We note that the randomly oriented MA or FA cations in the cages of the inorganic PbI_6/SnI_6 octahedra exhibit lower formation energies than highly ordered cations with a difference of ∼10 meV/atom.

Table 2: Calculated band gaps and charge–carrier effective masses of $(BA)_2A_{n-1}B_nI_{3n+1}$ materials, where A = MA or FA, B = Sn or Pb, and n = 1–4. The available experimental data are taken from Ref.[41] and Ref.[70] for Sn– and Pb–based systems, respectively.

System	n	Band gap (eV)			m_e^*/m_0	m_h^*/m_0
		PBEsol	PBEsol+SOC	exp.	in-plane	in–plane
$(BA)_2SnI_4$	1	1.10	0.82	1.83	0.12	-0.11
$(BA)_2MASn_2I_7$	2	0.73	0.53	1.64	0.12	-0.07
$(BA)_2(MA)_2Sn_3I_{10}$	3	0.58	0.35	1.50	0.09	-0.08
$(BA)_2(MA)_3Sn_4I_{13}$	4	0.56	0.34	1.42	0.10	-0.08
$(BA)_2FASn_2I_7$	2	0.78	0.55	–	0.07	-0.06
$(BA)_2(FA)_2Sn_3I_{10}$	3	0.62	0.42	–	0.09	-0.10
$(BA)_2(FA)_3Sn_4I_{13}$	4	0.57	0.35	–	0.10	-0.12
$(BA)_2PbI_4$	1	2.00	1.18	2.43	0.11	-0.13
$(BA)_2MAPb_2I_7$	2	1.82	0.94	2.17	0.14	-0.12
$(BA)_2(MA)_2Pb_3I_{10}$	3	1.58	0.72	2.03	0.09	-0.11
$(BA)_2(MA)_3Pb_4I_{13}$	4	1.56	0.69	1.91	0.08	-0.10
$(BA)_2FAPb_2I_7$	2	1.73	0.90	–	0.10	-0.13
$(BA)_2(FA)_2Pb_3I_{10}$	3	1.54	0.70	–	0.08	-0.12
$(BA)_2(FA)_3Pb_4I_{13}$	4	1.52	0.62	–	0.08	-0.09

3.2 Band gaps, effective masses, and Rashba effects

The 2D Pb– and Sn–based perovskites are all found to be semiconducting with a direct band gap character around the Γ point, independent of the number of layers n or the organic cation A (MA or FA). The band gap values, with and without SOC, are reported in Table 2, which indicate that the band gap decreases with increasing n and are consistent with the trends reported experimentally.[32,41,70] The calculated values are smaller than those obtained from experiment (see Table 2), as DFT is well–known to systematically underestimate band gaps, especially with the inclusion of spin-orbit interactions. In terms of trends, we find that for 2D Sn–based perovskites, the systems with FA cations exhibit slightly larger band gaps than their corresponding systems with MA cations. In contrast, for 2D Pb-based perovskites the opposite trend is observed, where the systems with FA cations have slightly smaller band gaps than those with MA cations with the same layer thickness n.

The charge-carrier effective masses along the in–plane directions of the 2D perovskites are almost isotropic and the averaged values are given in Table 2. Overall, the electron and hole effective masses of these 2D perovskites are comparable to the experimental reduced effective masses (0.10–0.12m_e) of $MAPbI_3$[73,74] and smaller than those calculated for 3D $MAPbI_3$ and $MASnI_3$, which are typically larger than 0.14m_e,[75,76] where m_e is the electron mass. These results suggest that 2D perovskites could exhibit higher charge-carrier mobilities. However, experimental measurements indicate that 2D perovskites displayed lower charge-carrier transport than the 3D perovskites.[77–79] This is likely due to the strong dielectric confinements associated with the small dielectric constants of the organic spacing layers, such as BA or PEA whose dielectric constants are 2.2[80] and 3.3,[81] respectively. This results in large exciton binding energies compared to 3D counterparts. Such binding energies hinder the dissociation of the excitons to form free charge-carriers via thermal excitation, which, in addition to quantum confinement effects, leads to

the observed low charge-carrier conduction.[77,82] Subsequently, it was suggested that a preferential vertical growth of the 2D perovskite crystals with respect to the substrate[49] or reducing the distance between the inorganic perovskite layers by using small alkylammonium cations[82,83] would lead to higher charge-carrier mobilities.[84] Table 2 shows that electron and hole effective masses are similar and vary only slightly with n for both Pb and Sn systems. For 2D Pb–based perovskites with $n > 1$, both electron and hole effective masses decrease slightly with the increase of the layer thickness n. For 2D Sn–based perovskites, no trend is observed for the systems containing the MA cations, whereas the effective masses of the systems with FA cations and $n > 1$ increase when the layer thickness n is increased. Our calculated effective masses corroborate a recent study, where they measured a hole mobility of 34 $cm^2 \cdot V^{-1} \cdot s^{-1}$ in a 2D Sn-based perovskite.[84]

The band structures of 2D Sn–based perovskites with MA and FA are plotted in Figures S1 and S2, respectively, with and without SOC for comparison. We find that the inclusion of SOC is important for obtaining accurate band dispersions as it has been shown that SOC associated with the symmetry properties and the orbital character of the bands have a significant effect on the band splittings, especially around the conduction band minimum (CBM) and the valence band maximum (VBM) at the Γ point.[85]

From the band structures with only SOC for 2D Sn–based perovskites shown in Figure 2, the systems with $n = 2$, 3, and 4 containing the MA cations display band splittings due to the Rashba effect in both conduction and valence band extrema. These Rashba band splittings are caused by the symmetry breaking in these distorted crystal structures. Yin et *al.*[86] investigated 2D Pb–based perovskites with phenethylammonium (PEA) as a spacing layer and $n = 1$, 2, and 3. They found that the Rashba splitting occurs only in the system with even number of layers ($n = 2$), whereas, the systems with odd number of layers ($n = 1$ and 3) show no band splitting since the centrosymmetry of the crystal structures is preserved. In our case, $(BA)_2SnI_4$ and $(BA)_2PbI_4$ have centrosymmetric crystal structures and, therefore, no Rashba band splitting is found. However, for $n > 1$, we believe that the interplay between the organic spacing molecules (BA) and the different orientations of the organic cations (MA or FA) in the perovskite layers induces a symmetry breaking in the Sn– and Pb–based structures.

We have assessed the effect of different orientations of the MA/FA cations in the inorganic layers, and find that when these cations are perfectly aligned (as shown in Figure 3-a), the systems do not exhibit any Rashba splitting. In contrast, when the FA cations are randomly oriented (shown in Figure 3-b), the systems display lower symmetry caused by the SnI_6/PbI_6 octahedra tilting, which yields the Rashba-type effect. The band splittings and the values of the Rashba parameters (α_R) are found to be dependent on the in-plane directions, in which the symmetry is broken. For example, the $(BA)_2MASn_2I_7$ system has a α_R of 0.30 eV·Å and a splitting energy of 7 meV along the $\Gamma-Z$ direction and α_R of 0.18 eV·Å and a splitting energy of 3 meV along the $\Gamma-X$ direction in the conduction band. As the content of the heavy elements (Sn, Pb, and I) increase with the thickness of the perovskite units, the splittings also become larger. For example, the system $(BA)_2MA_3Sn_4I_{13}$ exhibits a Rashba parameter α_R of 0.65 eV·Å with a splitting energy of 16 meV along the $\Gamma-Z$ direction. These values indicate that 2D perovskites display significant Rashba band splittings, which is in accord with experimental measurements on PEA_2PI_4 for which a Rashba parameter (α_R) of 1.6 eV·Å and an energy splitting of 40 meV have been reported.[87] For $(BA)_2(MA)_2Sn_3I_{10}$ and $(BA)_2(FA)_2Sn_3I_{10}$ systems, we find that the splittings are only along the $\Gamma-Z$ direction and are more significant in the conduction band than in the valence band.

One key finding induced by the Rashba effect in these 2D materials is that the splittings of the bands slightly shift the valence and conduction band extrema from the Γ point in the in-plane k-space and, therefore, the band gap adopts an indirect character. This, of course, could play

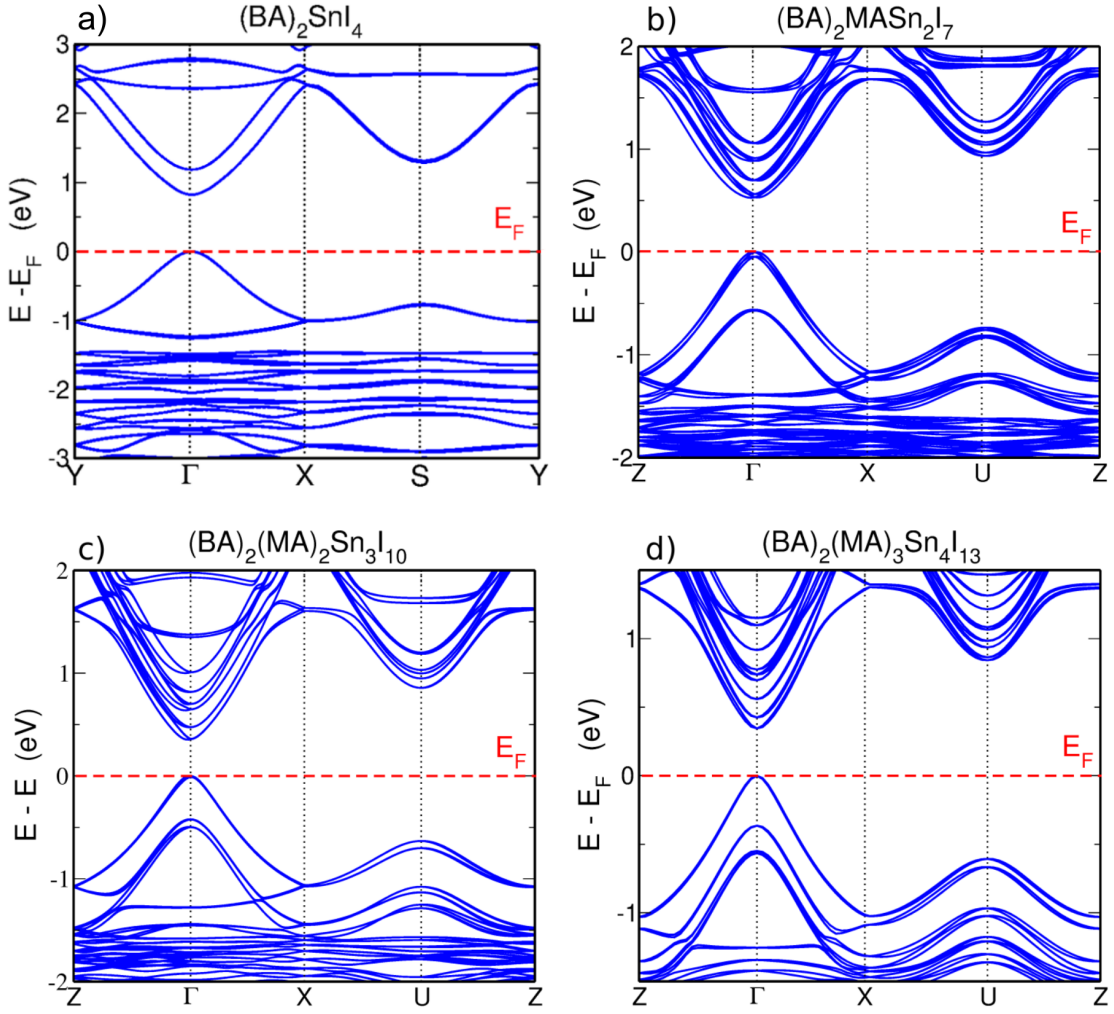

Figure 2: Band structures of $(BA)_2MA_{n-1}Sn_nI_{3n+1}$, for a) $n = 1$, b) $n = 2$, c) $n = 3$, and d) $n = 4$ obtained with PBEsol and SOC. We show the band structures along the k-path of the Brillouin zone that corresponds to the in–plane direction of the layers. The out–of–plane directions display flat bands and, therefore, are not included here.

an important role in the dynamics and the lifetimes of photo-generated carriers, for which the recombination process may be delayed by forbidden indirect transitions.

3.3 Interfaces and band alignment

The properties of interfaces in solar cells are crucial for their performance. Therefore, optimizing the energy level alignment between device components is one of the key factors for reducing non-radiative recombination and for efficient charge-carrier extraction and transfer, which would lead to improved photovoltages and power conversion efficiencies. However, the fundamental band alignment between 3D and 2D perovskites is not fully characterized.

We provide in Figure 4 the band alignment between the 3D perovskites (namely $MAPbI_3$, $FAPbI_3$, $MASnI_3$, and $FASnI_3$) and the 2D Sn– and Pb-based perovskites considered in this study. The level aligned is constructed based on the calculated work–functions (W) and band gaps using the PBE0 hybrid functional. It is noted that W coincides with the valence band maximum (VBM) of each material. We find that the VBMs and CBMs in the 2D perovskites increase with increasing n, ultimately converging to those of the 3D parent perovskites. This means that the transfer of photogenerated charge-carriers would go from $n = 1$ to

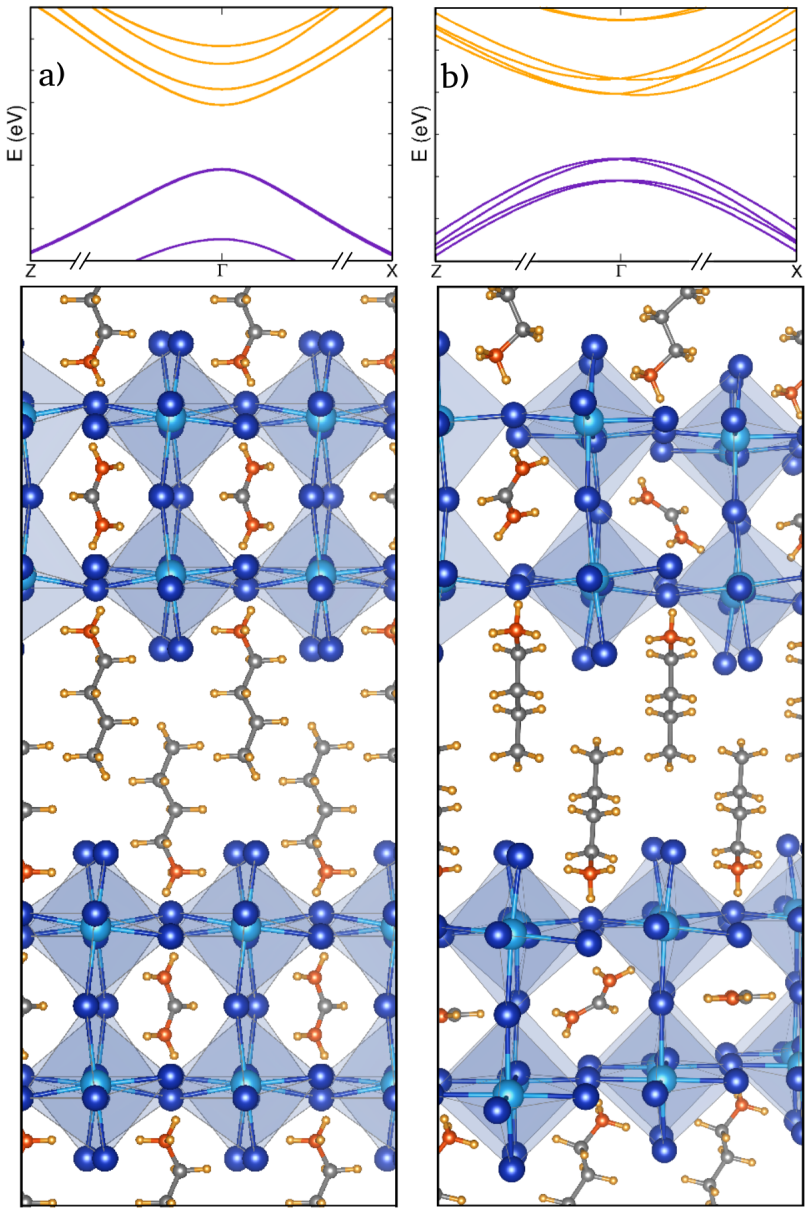

Figure 3: Rashba spin–splitting bands at the Γ point of the $(BA)_2FASn_2I_7$ structure with different FA orientations within the cages formed by the SnI_6 octahedra. a) Highly ordered FA cations show no splitting, b) randomly oriented FA cations show band splittings in both VBM and CBM.

$n = 4$ for electrons, but conversely from $n = 4$ to $n = 1$ for holes for both Sn and Pb materials with either MA or FA cations. These results are consistent with ultrafast transient absorption and photoluminescence measurements by Liu et *al.* on $(BA)_2(MA)_{n-1}Pb_nI_{3n+1}$, where they showed that the electron transfer proceeds from systems with smaller n to larger n and hole transfer in the opposite way.[88]

Figure 4 shows that the CBMs of the 2D perovskites are higher in energy than those of the 3D parents, whereas the VBMs of the 2D perovskites are located mainly between the band edges of the corresponding 3D perovskites. This suggests that the 2D perovskites would form staggered (type-II) heterojunctions with their 3D counterparts. Hence, when 2D perovskites are used alongside the 3D perovskites, they are prone to promote the hole extraction from the 3D materials and block the transfer of electrons.[89] These findings are in good agreement with ultraviolet photoelectron spectroscopy results on $(BA)_2(MA)_{n-1}Pb_nI_{3n+1}$ reported by Kanatzidis and co-workers,[40] in which the VBM

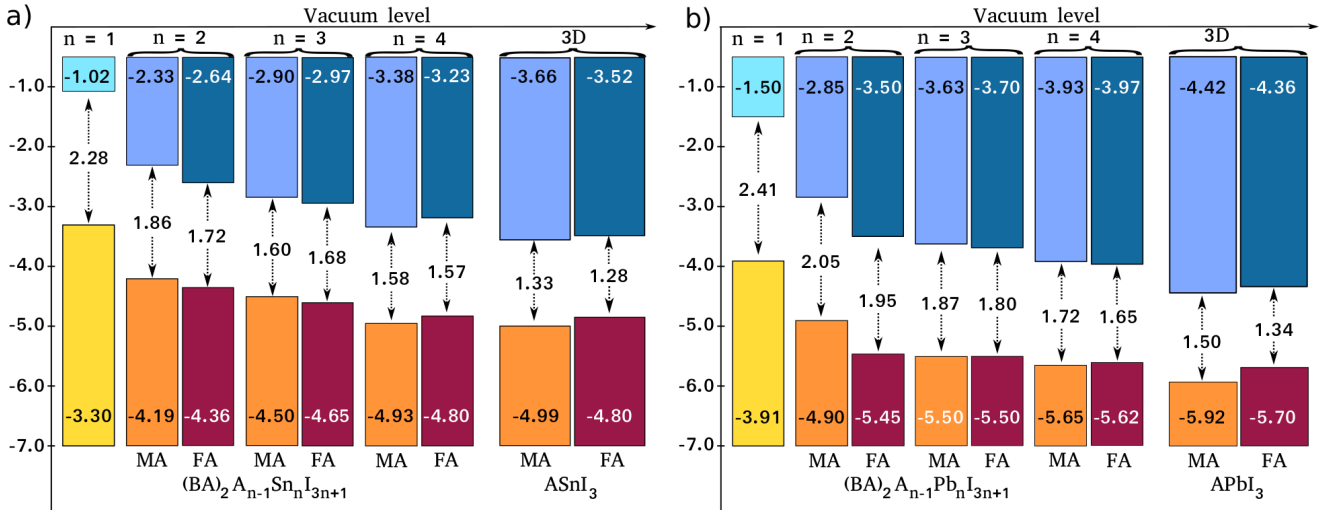

Figure 4: Energy band alignment between 2D and 3D perovskites (a) between $(BA)_2A_{n-1}Sn_nI_{3n+1}$ and ASn_nI_3, (b) between $(BA)_2A_{n-1}Pb_nI_{3n+1}$ and APb_nI , where A corresponds to MA^+ and FA^+ cations, and n = 1, 2, 3, and 4. The band gaps are in eV and the values in the boxes correspond to the band edge energies of each material (within an error of ±0.1 eV due to the convergence with the respect to slab thickness and the number of ghost functions used for the calculation of the work–functions[69]).

level of the 2D compounds goes upward with decreasing n in comparison to the VBM of $MAPbI_3$. Our calculated band gaps using the PBE0 functional for the Pb-based systems also agree well with their measured optical band gaps.[40] Similar observations are also reported by the same group on the 2D Sn-based perovskites.[41] The only exception is the system with a single layer ($n = 1$) that do not contain either MA or FA cations, namely $BASnI_4$ and $BAPbI_4$, for which the VBM levels are higher in energy than those of the 3D analogues. Accordingly, they would form a type-III heterojunction with a broken gap alongside the 3D perovskites. Hence, no charge extraction would be permitted from these 3D to the 2D single–layer systems.

Overall, the band alignment profiles indicate that these 2D perovskites can be used as hole transport layers (HTL) for the charge carrier extraction from the 3D analogues toward the contacts. However, reducing the nonradiative recombination and minimizing the photovoltage losses would depend on the number of layers n. It was shown that the open-circuit voltage (V_{oc}) depends highly on the energy difference between the CBM of the light absorber and the VBM of the HTL and the larger this difference the higher the V_{oc}.[90,91] Other effects, such as interfacial recombination, trap states, and interface defects, which play a role in the charge-carrier extraction would be similar in these materials. Consequently, our band level diagrams suggest that the 2D perovskites with larger number of layers n would result in higher V_{oc} than smaller n; for example, a 2D system with $n = 4$ would provide higer V_{oc} than 2D systems with $n = 2$ or $n = 1$. Therefore, efficient control of the material dimensionality with desirable thickness and adequate design of the device architecture would lead to improved photovoltaic performance of the mixed 3D/2D perovskite solar cells.

3.4 Conclusions

We have investigated the structural and electronic properties of 2D Sn– and Pb–based Ruddlesden–Popper perovskites $(BA)_2A_{n-1}B_nI_{3n+1}$ with butylammonium (BA) as a spacer and the number of layers (n) from 1 to 4, using density functional theory techniques. We have also examined the effect of substituting the MA with FA cations at the A site in the perovskite-like units.

First, the simulated crystal structures agree well with the available experimental parameters; the systems with even number of layers prefer low symmetry structures for both Sn and Pb materials with MA or FA cations. The calculated band gap progressively decreases with increasing layer thickness (n) for both Sn- and Pb-based materials, which is consistent with experimental trends. By replacing MA with FA cations in the perovskite units, the band gap slightly increases in the Sn systems, but decreases in the Pb systems. The electron and hole effective masses of these 2D perovskites are very light and smaller than those of the corresponding 3D perovskites, which suggest that these 2D compounds could exhibit high charge carrier mobilities.

Second, our band structure analysis indicates Rashba band splitting in the systems of $n > 1$ due to symmetry breaking in the distorted structures. However, the splitting magnitude is strongly associated with the orientation of the MA or FA cations and the degree of octahedra tilting in the perovskite units. For highly ordered MA or FA cations no band splitting is observed.

Finally, our band alignment diagrams indicate that the possible transfer process of photogenerated carriers in the 2D Ruddlesden–Popper perovskites goes from smaller to higher number of layers ($n = 1$ to 4) for electrons and in the opposite way for holes, which is in excellent accord with absorption and photoluminescence experiments. When 2D perovskites with $n > 1$ are used alongside 3D perovskites, they are expected to form staggered type-II heterojunctions that would promote hole charge extraction and transfer. In addition, 2D perovskites with a large number of layers are expected to deliver high open-circuit voltages in 2D/3D heterostructures. Hence, these 2D materials could be employed as efficient intrinsic hole transport layers.

Our findings provide new insights into understanding the structural and optoelectronic properties of both Sn– and Pb–based 2D perovskites and offer a possible route towards their integration into perovskite solar cell devices.

4 Notes

The authors declare no competing financial interest.

Acknowledgement The authors gratefully acknowledge the EPSRC Grant "Towards Self-scrubbing Stable and Scalable Perovskite Solar Cells" (EP/R020485/1). We thank the MCC/Archer consortium (EP/L000202/1) and Isambard UK National Tier-2 HPC Service operated by GW4 and the UK Met Office, and funded by EPSRC (EP/P020224/1) for supercomputer resources.

5 Supporting Information

Structural parameters of 2D Sn and Pb perovskites with FA cations, band structures of 2D Sn Perovskites with and without SOC, van der Waals corrections, computational details for conputing the work–function and the energy level alignment, HSE energy band alignment between $MAPbI_3$ and $(BA)_2MA_{n-1}Pb_nI_{n+1}$, crystal structures used in this work.

References

(1) Snaith, H. J. Present status and future prospects of perovskite photovoltaics. *Nature Materials* **2018**, *17*, 372–376.

(2) Akkerman, Q. A.; Rainò, G.; Kovalenko, M. V.; Manna, L. Genesis, challenges and opportunities for colloidal lead halide perovskite nanocrystals. *Nature Materials* **2018**, *17*, 394–405.

(3) Lin, Q.; Wang, Z.; Snaith, H. J.; Johnston, M. B.; Herz, L. M. Hybrid Perovskites: Prospects for Concentrator Solar Cells. *Adv. Sci.* **2018**, *5*, 1700792.

(4) National Renewable Energy Laboratory (NREL), Best Research-Cell Efficiencies Chart, https://www.nrel.gov/pv/cell-efficiency.html, accessed March 2020.

(5) Lin, Q.; Armin, A.; Burn, P. L.; Meredith, P. Organohalide Perovskites for So-

lar Energy Conversion. *Acc. Chem. Res.* **2016**, *49*, 545–553.

(6) Petrus, M. L.; Schlipf, J.; Li, C.; Gujar, T. P.; Giesbrecht, N.; Müller-Buschbaum, P.; Thelakkat, M.; Bein, T.; Hüttner, S.; Docampo, P. Capturing the Sun: A Review of the Challenges and Perspectives of Perovskite Solar Cells. *Adv. Energy Mater.* **2017**, *7*, 1700264.

(7) Rosales, B. A.; Hanrahan, M. P.; Boote, B. W.; Rossini, A. J.; Smith, E. A.; Vela, J. Lead Halide Perovskites: Challenges and Opportunities in Advanced Synthesis and Spectroscopy. *ACS Energy Lett.* **2017**, *2*, 906–914.

(8) Babayigit, A.; Duy Thanh, D.; Ethirajan, A.; Manca, J.; Muller, M.; Boyen, H.-G.; Conings, B. Assessing the toxicity of Pb- and Sn-based perovskite solar cells in model organism Danio rerio. *Scientific Reports* **2016**, *6*, 18721.

(9) Benmessaoud, I. R.; Mahul-Mellier, A.-L.; Horváth, E.; Maco, B.; Spina, M.; Lashuel, H. A.; Forró, L. Health hazards of methylammonium lead iodide based perovskites: cytotoxicity studies. *Toxicol. Res.* **2016**, *5*, 407–419.

(10) Zarick, H. F.; Soetan, N.; Erwin, W. R.; Bardhan, R. Mixed halide hybrid perovskites: a paradigm shift in photovoltaics. *J. Mater. Chem. A* **2018**, *6*, 5507–5537.

(11) Ono, L. K.; Park, N.-G.; Zhu, K.; Huang, W.; Qi, Y. Perovskite Solar Cells–Towards Commercialization. *ACS Energy Lett.* **2017**, *2*, 1749–1751
.

(12) Kumar, M. H.; Dharani, S.; Leong, W. L.; Boix, P. P.; Prabhakar, R. R.; Baikie, T.; Shi, C.; Ding, H.; Ramesh, R.; Asta, M.; Graetzel, M.; Mhaisalkar, S. G.; Mathews, N. Lead-Free Halide Perovskite Solar Cells with High Photocurrents Realized Through Vacancy Modulation. *Adv. Mater.* **2014**, *26*, 7122–7127
.

(13) Abate, A. Perovskite Solar Cells Go Lead Free. *Joule* **2017**, *1*, 659–664.

(14) Shao, S.; Liu, J.; Portale, G.; Fang, H.-H.; Blake, G. R.; ten Brink, G. H.; Koster, L. J. A.; Loi, M. A. Highly Reproducible Sn-Based Hybrid Perovskite Solar Cells with 9% Efficiency. *Adv. Energy Mater.* **2018**, *8*, 1702019.

(15) Liu, C.; Li, W.; Fan, J.; Mai, Y. A brief review on the lead element substitution in perovskite solar cells. *Journal of Energy Chemistry* **2018**, 1054–1066.

(16) Liu, X.; Yan, K.; Tan, D.; Liang, X.; Zhang, H.; Huang, W. Solvent Engineering Improves Efficiency of Lead-Free Tin-Based Hybrid Perovskite Solar Cells beyond 9%. *ACS Energy Lett.* **2018**, *3*, 2701–2707.

(17) Zimmermann, I.; Aghazada, S.; Nazeeruddin, M. K. Lead and HTM Free Stable Two-Dimensional Tin Perovskites with Suitable Band Gap for Solar Cell Applications. *Angew. Chem. Int. Ed.* **2019**, *58*, 1072–1076.

(18) Stoumpos, C. C. Tin Perovskite Solar Cells Are Back in the Game. *Joule* **2018**, *2*, 2517–2518.

(19) Kayesh, M. E.; Matsuishi, K.; Kaneko, R.; Kazaoui, S.; Lee, J.-J.; Noda, T.; Islam, A. Coadditive Engineering with 5-Ammonium Valeric Acid Iodide for Efficient and Stable Sn Perovskite Solar Cells. *ACS Energy Lett.* **2019**, *4*, 278–284.

(20) Jokar, E.; Chien, C.-H.; Tsai, C.-M.; Fathi, A.; Diau, E. W.-G. Robust Tin-Based Perovskite Solar Cells with Hybrid Organic Cations to Attain Efficiency Approaching 10%. *Adv. Mater.* **2019**, *31*, 1804835.

(21) Diau, E. W.-G.; Jokar, E.; Rameez, M. Strategies To Improve Performance and Stability for Tin-Based Perovskite Solar

Cells. *ACS Energy Lett.* **2019**, *4*, 1930–1937.

(22) Lin, J.-T.; Liao, C.-C.; Hsu, C.-S.; Chen, D.-G.; Chen, H.-M.; Tsai, M.-K.; Chou, P.-T.; Chiu, C.-W. Harnessing Dielectric Confinement on Tin Perovskites to Achieve Emission Quantum Yield up to 21**2019**, *141*, 10324–10330.

(23) Fu, H. Review of lead-free halide perovskites as light-absorbers for photovoltaic applications: From materials to solar cells. *Solar Energy Materials and Solar Cells* **2019**, *193*, 107–132.

(24) Zhang, Q.; Ting, H.; Wei, S.; Huang, D.; Wu, C.; Sun, W.; Qu, B.; Wang, S.; Chen, Z.; Xiao, L. Recent progress in lead-free perovskite (-like) solar cells. *Materials Today Energy* **2018**, *8*, 157–165
.

(25) Liu, G.; Zheng, H.; Xu, X.; Xu, S.; Zhang, X.; Pan, X.; Dai, S. Introduction of Hydrophobic Ammonium Salts with Halogen Functional Groups for High-Efficiency and Stable 2D/3D Perovskite Solar Cells. *Adv. Funct. Mater.* **2019**, *29*, 1807565.

(26) He, Q.; Worku, M.; Xu, L.; Zhou, C.; Lin, H.; Robb, A. J.; Hanson, K.; Xin, Y.; Ma, B. Facile Formation of 2D-3D Heterojunctions on Perovskite Thin Film Surfaces for Efficient Solar Cells. *ACS Appl. Mater. Interfaces* **2020**, *12*, 1159–1168
.

(27) Chen, K.; Wu, P.; Yang, W.; Su, R.; Luo, D.; Yang, X.; Tu, Y.; Zhu, R.; Gong, Q. Low-dimensional perovskite interlayer for highly efficient lead-free formamidinium tin iodide perovskite solar cells. *Nano Energy* **2018**, *49*, 411–418.

(28) Chen, Z.; Liu, M.; Li, Z.; Shi, T.; Yang, Y.; Yip, H.-L.; Cao, Y. Stable Sn/Pb-Based Perovskite Solar Cells with a Coherent 2D/3D Interface. *iScience* **2018**, *9*, 337–346.

(29) Li, L.; Zhou, N.; Chen, Q.; Shang, Q.; Zhang, Q.; Wang, X.; Zhou, H. Unraveling the Growth of Hierarchical Quasi-2D/3D Perovskite and Carrier Dynamics. *J. Phys. Chem. Lett.* **2018**, *9*, 1124–1132
.

(30) Niu, T.; Lu, J.; Tang, M.-C.; Barrit, D.; Smilgies, D.-M.; Yang, Z.; Li, J.; Fan, Y.; Luo, T.; McCulloch, I.; Amassian, A.; Liu, S. F.; Zhao, K. High performance ambient–air–stable FAPbI3 perovskite solar cells with molecule–passivated Ruddlesden–Popper/3D heterostructured film. *Energy Environ. Sci.* **2018**, *11*, 3358–3366
.

(31) Ishihara, T.; Takahashi, J.; Goto, T. Optical properties due to electronic transitions in two-dimensional semiconductors $(C_nH_{2n+1}NH_3)_2PbI_4$. *Phys. Rev. B* **1990**, *42*, 11099–11107.

(32) Mitzi, D. B.; Feild, C. A.; Harrison, W. T. A.; Guloy, A. M. Conducting Tin Halides with a Layered Organic-Based Perovskite Structure. *Nature* **1994**, *369*, 467–469 .

(33) Mitzi, D. B.; Wang, S.; Feild, C. A.; Chess, C. A.; Guloy, A. M. Conducting Layered Organic–Inorganic Halides Containing ⟨110⟩–Oriented Perovskite Sheets. *Science* **1995**, *267*, 1473– 1476.

(34) Mitzi, D. B. Synthesis, Structure, and Properties of Organic-Inorganic Perovskites and Related Materials. *In Progress in Inorganic Chemistry, K.D. Karlin (Ed.)*; John Wiley & Sons, Ltd, 2007; 1–121.

(35) Ma, L.; Ju, M.-G.; Dai, J.; Zeng, X. C. Tin and germanium based two-dimensional Ruddlesden-Popper hybrid perovskites for potential lead-free photovoltaic and photoelectronic applications. *Nanoscale* **2018**, *10*, 11314–11319.

(36) Tsai, H.; Asadpour, R.; Blancon, J.-C.; Stoumpos, C. C.; Even, J.; Ajayan, P. M.;

Kanatzidis, M. G.; Alam, M. A.; Mohite, A. D.; Nie, W. Design principles for electronic charge transport in solution-processed vertically stacked 2D perovskite quantum wells. *Nature Communications* **2018**, *9*, 2130.

(37) Zhang, Z.; Fang, W.-H.; Tokina, M. V.; Long, R.; Prezhdo, O. V. Correction for Rapid Decoherence Suppresses Charge Recombination in Multilayer 2D Halide Perovskites: Time-Domain Ab Initio Analysis. *Nano Lett.* **2018**, *18*, 3312–3312.

(38) Venkatesan, N. R.; Labram, J. G.; Chabinyc, M. L. Charge-Carrier Dynamics and Crystalline Texture of Layered Ruddlesden-Popper Hybrid Lead Iodide Perovskite Thin Films. *ACS Energy Lett.* **2018**, *3*, 380–386
.

(39) Park, I.-H.; Chu, L.; Leng, K.; Choy, Y. F.; Liu, W.; Abdelwahab, I.; Zhu, Z.; Ma, Z.; Chen, W.; Xu, Q.-H.; Eda, G.; Loh, K. P.; Highly Stable Two-Dimensional Tin(II) Iodide Hybrid Organic-Inorganic Perovskite Based on Stilbene Derivative. *Adv. Funct. Mater.* **2019**, *29*, 1904810
.

(40) Cao, D. H.; Stoumpos, C. C.; Farha, O. K.; Hupp, J. T.; Kanatzidis, M. G. 2D Homologous Perovskites as Light-Absorbing Materials for Solar Cell Applications. *J. Am. Chem. Soc.* **2015**, *137*, *24*, 7843–7850.

(41) Cao, D. H.; Stoumpos, C. C.; Yokoyama, T.; Logsdon, J. L.; Song, T.-B.; Farha, O. K.; Wasielewski, M. R.; Hupp, J. T.; Kanatzidis, M. G. Thin Films and Solar Cells Based on Semiconducting Two-Dimensional Ruddlesden-Popper $(CH_3(CH_2)_3NH_3)_2(CH_3NH_3)_{n-1}Sn_nI_{3n+1}$ Perovskites. *ACS Energy Lett.* **2017**, *2*, 982–990
.

(42) Liao, Y.; Liu, H.; Zhou, W.; Yang, D.; Shang, Y.; Shi, Z.; Li, B.; Jiang, X.; Zhang, L.; Quan, L. N.; Quintero-Bermudez, R.; Sutherland, B. R.; Mi, Q.; Sargent, E. H.; Ning, Z. Highly Oriented Low-Dimensional Tin Halide Perovskites with Enhanced Stability and Photovoltaic Performance. *J. Am. Chem. Soc.* **2017**, *139*, *19*, 6693–6699
.

(43) Ke, W.; Stoumpos, C. C.; Kanatzidis, M. G. "Unleaded" Perovskites: Status Quo and Future Prospects of Tin-Based Perovskite Solar Cells. *Adv. Mater.* **2018**, 1803230.

(44) Lai, H.; Kan, B.; Liu, T.; Zheng, N.; Xie, Z.; Zhou, T.; Wan, X.; Zhang, X.; Liu, Y.; Chen, Y. Two–Dimensional Ruddlesden–Popper Perovskite with Nanoro–like Morphology for Solar Cells with Efficiency Exceeding 15%. *Journal of the American Chemical Society* **2018**, *140*, *37*, 11639–11646.

(45) Ma, S.; Cai, M.; Cheng, T.; Ding, X.; Shi, X.; Alsaedi, A.; Hayat, T.; Ding, Y.; Tan, Z.; Dai, S. Two-dimensional organic-inorganic hybrid perovskite: from material properties to device applications. *Science China Materials* **2018**, *61*, 1257–1277.

(46) Mao, L.; Stoumpos, C. C.; Kanatzidis, M. G. Two-Dimensional Hybrid Halide Perovskites: Principles and Promises. *Journal of the American Chemical Society* **2019**, *141*, 1171–1190
.

(47) Spanopoulos, I.; Hadar, I.; Ke, W.; Tu, Q.; Chen, M.; Tsai, H.; He, Y.; Shekhawat, G.; Dravid, V. P.; Wasielewski, M. R.; Mohite, A. D.; Stoumpos, C. C.; Kanatzidis, M. G. Uniaxial Expansion of the 2D Ruddlesden-Popper Perovskite Family for Improved Environmental Stability. *J. Am. Chem. Soc.* **2019**, *141*, *13*, 5518–5534
.

(48) Smith, I. C.; Hoke, E. T.; Solis-Ibarra, D.; McGehee, M. D.; Karunadasa, H. I. A Layered Hybrid Perovskite Solar-Cell Absorber with Enhanced Moisture Stability. *Angew. Chem., Int. Ed.* **2014**, *126*, 11414–11417
.

(49) Tsai, H.; Nie, W.; Blancon, J.-C.; Stoumpos, C. C.; Asadpour, R.; Harutyunyan, B.; Neukirch, A. J.; Verduzco, R.; Crochet, J. J.; Tretiak, S. Pedesseau, L.; Even, J.; Alam, M. A.; Gupta, G.; Lou, J.; Ajayan, P. M.; Bedzyk, M. J.; Kanatzidis, M. G.; Mohite, A. D. High-efficiency two-dimensional Ruddlesden–Popper perovskite solar cells. *Nature* **2016**, *536*, 312–316
.

(50) Zheng, H.; Liu, G.; Zhu, L.; Ye, J.; Zhang, X.; Alsaedi, A.; Hayat, T.; Pan, X.; Dai, S. The Effect of Hydrophobicity of Ammonium Salts on Stability of Quasi-2D Perovskite Materials in Moist Condition. *Advanced Energy Materials* **2018**, *8*, 1800051.

(51) Wang, Z.; Lin, Q.; Chmiel, F. P.; Sakai, N.; Herz, L. M.; Snaith, H. J. Efficient ambient-air-stable solar cells with 2D–3D heterostructured butylammonium-caesium-formamidinium lead halide perovskites. *Nat. Energy* **2017**, *2*, 17135.

(52) Aristidou, N.; Eames, C.; Sanchez-Molina, I.; Bu, X.; Kosco, J.; Islam, M. S.; Haque, S. A. Fast oxygen diffusion and iodide defects mediate oxygen-induced degradation of perovskite solar cells. *Nature Communications* **2017**, *8*, 15218.

(53) Ghosh, D.; Smith, A. R.; Walker, A. B.; Islam, M. S. Mixed A-Cation Perovskites for Solar Cells: Atomic-Scale Insights Into Structural Distortion, Hydrogen Bonding, and Electronic Properties. *Chem. Mater.* **2018**, *30*, 5194–5204.

(54) Nagane, S.; Ghosh, D.; Hoye, R. L. Z.; Zhao, B.; Ahmad, S.; Walker, A. B.; Islam, M. S.; Ogale, S.; Sadhanala, A. Lead-Free Perovskite Semiconductors Based on Germanium-Tin Solid Solutions: Structural and Optoelectronic Properties. *J. Phys. Chem. C* **2018**, *122*, 5940.

(55) Brenes, R.; Eames, C.; Bulović, V.; Islam, M. S.; Stranks, S. D. The Impact of Atmosphere on the Local Luminescence Properties of Metal Halide Perovskite Grains. *Adv. Mater.* **2018**, *30*, 1706208.

(56) Lee, J.-W.; Seol, D.-J.; Cho, A.-N.; Park, N.-G. High-Efficiency Perovskite Solar Cells Based on the Black Polymorph of HC(NH2)2PbI3. *Adv. Mater.* **2014**, *26*, 4991–4998.

(57) Koh, T. M.; Krishnamoorthy, T.; Yantara, N.; Shi, C.; Leong, W. L.; Boix, P. P.; Grimsdale, A. C.; Mhaisalkar, S. G.; Mathews, N. Formamidinium tin-based perovskite with low Eg for photovoltaic applications. *J. Mater. Chem. A* **2015**, *3*, 14996–15000.

(58) Kohn, W.; Sham, L. J. Self-Consistent Equations Including Exchange and Correlation Effects. *Phys. Rev.* **1965**, *140*, A1133–A1138
.

(59) Giannozzi, P.; Andreussi, O.; Brumme, T.; Bunau, O.; Nardelli, M. B.; Calandra, M.; Car, R.; Cavazzoni, C.; Ceresoli, D.; Cococcioni, M. Colonna, N.; Carnimeo, I.; Dal Corso, A.; de Gironcoli, S.; Delugas, P.; DiStasio Jr., R. A.; Ferretti, A.; Floris A.; Fratesi, G.; Fugallo, G.; Gebauer, R.; Gerstmann, U.; Giustino, F.; Gorni, T.; Jia, J.; Kawamura, M.; Ko, H.–Y.; Kokalj, A.; Küçükbenli, E.; Lazzeri, M.; Marsili, M.; Marzari, N.; Mauri, F.; Nguyen, N. L.; Nguyen, H.–V.; Otero–de–la-Roza, A.; Paulatto, L.; Poncé, S.; Rocca, D.; Sabatini, R.; Santra, B.; Schlipf, M.; Seitsonen, A. P.; Smogunov, A.; Timrov, I.;

Thonhauser, T.; Umari, P.; Vast, N.; Wu, X.; Baroni, S. Advanced capabilities for materials modelling with Q uantum ESPRESSO. *Journal of Physics: Condensed Matter* **2017**, *29*, 465901
.

(60) Giannozzi, P.; Baroni, S.; Bonini, N.; Calandra, M.; Car, R.; Cavazzoni, C.; Ceresoli, D.; Chiarotti, G. L.; Cococcioni, M.; Dabo, I. Quantum Espresso: A Modular and Open-Source Software Project for Quantum Simulations Of Materials. *J. Phys.: Condens. Matter* **2009**, *21*, 395502.

(61) Perdew, J. P.; Ruzsinszky, A.; Csonka, G. I.; Vydrov, O. A.; Scuseria, G. E.; Constantin, L. A.; Zhou, X.; Burke, K. Restoring the Density-Gradient Expansion for Exchange in Solids and Surfaces. *Phys. Rev. Lett.* **2008**, *100*, 136406.

(62) Vanderbilt, D. Soft Self-Consistent Pseudopotentials in a Generalized Eigenvalue Formalism. *Phys. Rev. B* **1990**, *41*, 7892–7895.

(63) Rappe, A. M.; Rabe, K. M.; Kaxiras, E.; Joannopoulos, J. D. Optimized Pseudopotentials. *Phys. Rev. B* **1990**, *41*, 1227–1230.

(64) Monkhorst, H. J.; Pack, J. D. Special points for Brillouin-zone integrations. *Phys. Rev. B* **1976**, *13*, 5188–5192.

(65) Perdew, J. P.; Ernzerhof, M.; Burke, K. Rationale for mixing exact exchange with density functional approximations. *J.Chem. Phys.* **1996**, *105*, 9982–9985.

(66) Adamo, C.; Barone, V. Toward reliable density functional methods without adjustable parameters: The PBE0 model. *J. Chem. Phys.* **1999**, *110*, 6158–6170.

(67) Chen, W.; Pasquarello, A. Band-edge levels in semiconductors and insulators: Hybrid density functional theory versus many-body perturbation theory. *Phys. Rev. B* **2012**, *86*, 035134
.

(68) Dovesi, R.; Erba, A.; Orlando, R.; Zicovich-Wilson, C. M.; Civalleri, B.; Maschio, L.; Rérat, M.; Casassa, S.; Baima, J.; Salustro, S.; Kirtman, B. Quantum-mechanical condensed matter simulations with CRYSTAL. *WIREs Comput Mol Sci* **2018**, *8*, e1360
.

(69) Doll, K. Calculation of the work function with a local basis set. *Surface Science* **2006**, *600*, L321–L325.

(70) Stoumpos, C. C.; Cao, D. H.; Clark, D. J.; Young, J.; Rondinelli, J. M.; Jang, J. I.; Hupp, J. T.; Kanatzidis, M. G. Ruddlesden-Popper Hybrid Lead Iodide Perovskite 2D Homologous Semiconductors. *Chem. Mater.* **2016**, *28*, 2852.

(71) Ono, L. K.; Juarez-Perez, E. J.; Qi, Y. Progress on Perovskite Materials and Solar Cells with Mixed Cations and Halide Anions. *ACS Appl. Mater. Interfaces* **2017**, *9*, 30197–30246.

(72) Wang, Z.; Ganose, A.; Niu, C.; Scanlon, D. O. First-principles insights into tin-based two-dimensional hybrid halide perovskites for photovoltaics. *J. Mater. Chem. A* **2018**, *6*, 5652–5660.

(73) Hirasawa, M.; Ishihara, T.; Goto, T.; Uchida, K.; Miura, N. Magnetoabsorption of the lowest exciton in perovskite-type compound (CH3NH3)PbI3. *Physica B: Condensed Matter* **1994**, *201*, 427–430.

(74) Miyata, A.; Mitioglu, A.; Plochocka, P.; Portugall, O.; Wang, J. T.-W.; Stranks, S. D.; Snaith, H. J.; Nicholas, R. J. Direct measurement of the exciton binding energy and effective masses for charge carriers in organic-inorganic tri-halide perovskites. *Nature Physics* **2015**, *11*, 582–587.

(75) Umari, P.; Mosconi, E.; De Angelis, F. Relativistic GW Calculations on $CH_3NH_3PbI_3$ and $CH_3NH_3SnI_3$ Perovskites for Solar Cell Applications. *Sci. Rep.* **2014**, *4*, 4467.

(76) Davies, C. L.; Filip, M. R.; Patel, J. B.; Crothers, T. W.; Verdi, C.; Wright, A. D.; Milot, R. L.; Giustino, F.; Johnston, M. B.; Herz, L. M. Bimolecular recombination in methylammonium lead triiodide perovskite is an inverse absorption process. *Nat. Commun.* **2018**, *9*, 293.

(77) Milot, R. L.; Sutton, R. J.; Eperon, G. E.; Haghighirad, A. A.; Martinez Hardigree, J.; Miranda, L.; Snaith, H. J.; Johnston, M. B.; Herz, L. M. Charge-Carrier Dynamics in 2D Hybrid Metal–Halide Perovskites. *Nano Lett.* **2016**, *16*, *11*, 7001–7007.

(78) Saparov, B.; Mitzi, D. B. Organic–Inorganic Perovskites: Structural Versatility for Functional Materials Design. *Chem. Rev.* **2016**, *116*, *7*, 4558–4596.

(79) Herz, L. M. Charge-Carrier Mobilities in Metal Halide Perovskites: Fundamental Mechanisms and Limits. *ACS Energy Lett.* **2017**, *2*, 1539–1548
.

(80) Blancon, J. C.; Stier, A. V.; Tsai, H.; Nie, W.; Stoumpos, C. C.; Traoré, B.; Pedesseau, L.; Kepenekian, M.; Katsutani, F.; Noe, G. T. Kono, J.; Tretiak, S.; Crooker, S. A.; Katan, C.; Kanatzidis, M. G.; Crochet, J. J.; Even, J.; Mohite, A. D. Scaling law for excitons in 2D perovskite quantum wells. *Nat. Commun.* **2018**, *9*, 2254
.

(81) Hong, X.; Ishihara, T.; Nurmikko, A. V. Dielectric confinement effect on excitons in PbI4-based layered semiconductors. *Phys. Rev. B.* **1992**, *45*, 6961–6964
.

(82) Ma, C.; Shen, D.; Ng, T.-W.; Lo, M.-F.; Lee, C.-S. 2D Perovskites with Short Interlayer Distance for High-Performance Solar Cell Application. *Adv. Mater.* **2018**, *30*, 1800710
.

(83) Venkatesan, N. R.; Mahdi, A.; Barraza, B.; Wu, G.; Chabinyc, M. L.; Seshadri, R. Enhanced yield-mobility products in hybrid halide Ruddlesden-Popper compounds with aromatic ammonium spacers. *Dalton Trans.* **2019**, *48*, 14019–14026
.

(84) Shen, H.; Li, J.; Wang, H.; Ma, J.; Wang, J.; Luo, H.; Li, D. Two-Dimensional Lead-Free Perovskite (C6H5C2H4NH3)2CsSn2I7 with High Hole Mobility. *J. Phys. Chem. Lett.* **2019**, *10*, *1*, 7–12
.

(85) Even, J.; Pedesseau, L.; Dupertuis, M. A.; Jancu, J. M.; Katan, C. Electronic Model for Self-Assembled Hybrid Organic/Perovskite Semiconductors: Reverse Band Edge Electronic States Ordering and Spin-Orbit Coupling. *Phys. Rev. B* **2012**, *86*, 205301.

(86) Yin, J.; Maity, P.; Xu, L.; El-Zohry, A. M.; Li, H.; Bakr, O. M.; Brédas, J.-L.; Mohammed, O. F. Layer-Dependent Rashba Band Splitting in 2D Hybrid Perovskites. *Chem. Mater.* **2018**, *30*, 8538–8545.

(87) Zhai, Y.; Baniya, S.; Zhang, C.; Li, J.; Haney, P.; Sheng, C.-X.; Ehrenfreund, E.; Vardeny, Z. V. Giant Rashba splitting in 2D organic-inorganic halide perovskites measured by transient spectroscopies. *Sci Adv* **2017**, *3*, e1700704.

(88) Liu, J.; Leng, J.; Wu, K.; Zhang, J.; Jin, S. Observation of Internal Photoinduced Electron and Hole Separation in Hybrid Two-Dimentional Perovskite Films. *J. Am. Chem. Soc.* **2017**, *139*, *4*, 1432–1435
.

(89) Shao, Y.; Liu, Y.; Chen, X.; Chen, C.; Sarpkaya, I.; Chen, Z.; Fang, Y.; Kong, J.; Watanabe, K.; Taniguchi, T.; Taylor, A.; Huang, J.; Xia, F. Stable Graphene-Two-Dimensional Multiphase Perovskite Heterostructure Phototransistors with High Gain. *Nano Lett.* **2017**, *17*, *12*, 7330–7338 .

(90) Ompong, D.; Singh, J. High open-circuit voltage in perovskite solar cells: The role of hole transport layer. *Organic Electronics* **2018**, *63*, 104–108 .

(91) Stolterfoht, M.; Caprioglio, P.; Wolff, C. M.; Márquez, J. A.; Nordmann, J.; Zhang, S.; Rothhardt, D.; Hörmann, U.; Amir, Y.; Redinger, A. Kegelmann, L.; Zu, F.; Albrecht, S.; Koch, N.; Kirchartz, T.; Saliba, M.; Unold, T.; Neher, D. The impact of energy alignment and interfacial recombination on the internal and external open-circuit voltage of perovskite solar cells. *Energy Environ. Sci.* **2019**, *12*, 2778–2788 .

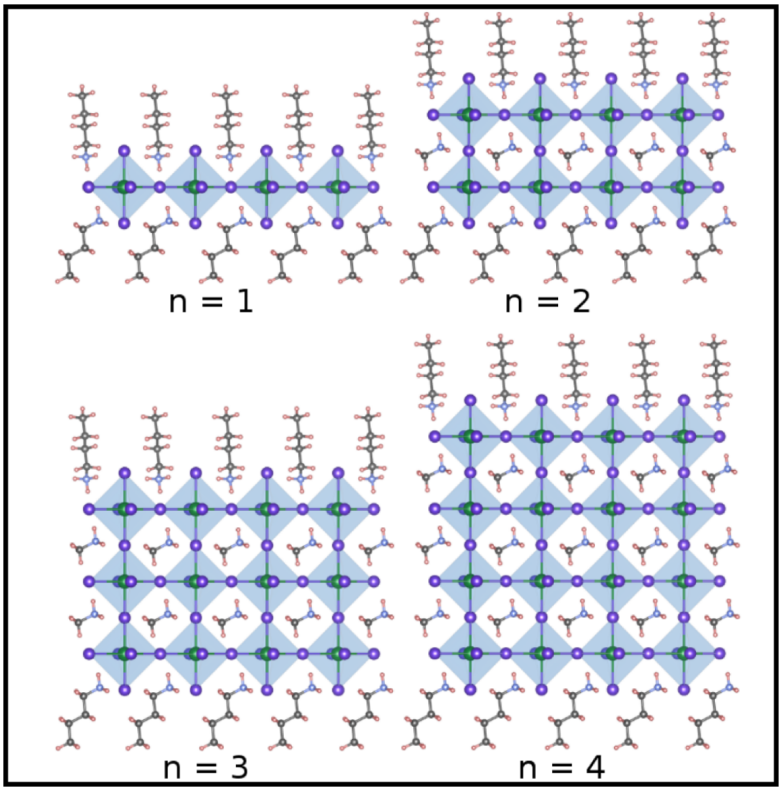

TOC Graphic